J. Ind. Geophys. Union, 29(2) (2025), 68-80

Geochemical constraints on the origin of ophiolitic chert from Naga Hills Ophiolite, Northeast India

Anisha Verencar[1,2], Abhishek Saha[1*], M. Ram Mohan[3]
[1]CSIR-National Institute of Oceanography, Dona Paula, Goa-403 004, India
[2]School of Earth, Ocean and Atmospheric Sciences, Goa University, Taleigão Plateau, Goa-403 206, India
[3]CSIR-National Geophysical Research Institute, Uppal Road, Hyderabad-500 007, India
*Corresponding author: asaha.nio2015@gmail.com

ABSTRACT

The uppermost part of the Naga Hills ophiolite (NHO) sequence representing vestiges of the Neo-Tethyan ocean in the Indo-Myanmar ranges, consists of Late Jurassic to Late Cretaceous cherts that carapace the ophiolitic volcanics. This contribution presents petrographic and whole rock geochemical studies to comprehend their origin and paleo-depositional environment. The occurrences of abundant radiolarian microfossils in the studied cherts are observed. Geochemical signatures of these cherts indicate that they are generated at rifted arc basin by pronounced hydrothermal activity along with terrigenous material influx from active continental margin. Redox sensitive trace element proxies U/Th (0.12-0.74), Ni/Co (0.10-0.67) and V/(V+Ni) (0.22-0.47) record oxic paleo-redox conditions of formation. The cherts of NHO are envisaged to have formed in a transitional tectonic environment associated with magmatism and subsequent sedimentation in a rifted arc basin proximal to an active continental margin.

Keywords: Ophiolite, Radiolarian chert, Depositional environment, Paleo-redox conditions, Tethys Ocean.

INTRODUCTION

The north eastern extension of the Yarlung-Tsangpo suture zone, located along the Indo-Myanmar ranges (IMR), hosts a collage of dismembered ophiolitic suite and mélange of Neo-Tethyan origin. This ophiolitic suite comprising plutonic to volcanic lithologies of ultramafic-mafic composition, is overlain by deep sea silicious pelagic sediments with radiolarian fossils. The Naga Hills ophiolite (NHO), the northern most extension of the IMR, hosts a dismembered suite of ophiolitic rocks. Many workers have discussed different tectonic settings for the formation of NHO from mineral chemical and whole rock studies of one or more litho-units belonging to this ophiolitic suite and associated metamorphic complex. Early works suggest basalts to be originated in a back arc basin environment, while some suggest within plate tectonic regime for their origin (Sengupta et al., 1989; Rao et al., 2010). Recent studies suggest dual affinities for the NHO i.e. mid oceanic ridge and arc tectonic setting (Dey et al., 2018; Hussain and Dey, 2022). Singh et al. (2016) and Khogenkumar et al. (2021) suggest both non-subduction (viz. OIB and MORB) and subduction origin. Studies based on the metamorphic complex associated with the NHO, reveal that the basalts were metamorphosed to blueschist and eclogite facies in a subduction zone setting (Chatterjee and Ghose, 2010; Ao and Bhowmik, 2014; Bhowmik et. al, 2022; Bhowmik and Pradhan, 2024). Our previous works based on the spinel chemistry and whole rock Os isotopic studies for mafic-ultramafic plutonic assemblage of NHO, indicates the evolution of the NHO to a supra-subduction zone tectonic setting (Verencar et al., 2021; 2022; 2024a).

The chert beds are largely intercalated with the mafic volcanics of the NHO and these have been least studied as compared to their igneous counterparts in the ophiolitic sequence. The geochemical studies of these siliceous rocks containing radiolarians and sponge spicules, have become an important tool to infer the paleogeography and the tectonic setting of their depositional environment. Certain major oxides like TiO_2, Al_2O_3, Fe_2O_3 and MnO in addition to trace and rare earth elements, have been effectively used to evaluate the process involved in the genesis of cherts (Kato et al., 2002; Huang et al., 2013; Garbán et al., 2017). A few studies including paleontological studies by Agrawal (1985) and Baxter et al. (2011); and geochemical studies by Thong et al. (2022) have been carried out earlier on the cherts from NHO. Here, in this study, we evaluate the geochemical signatures of the cherts associated with ophiolitic volcanic rocks and further discuss their depositional environment in terms of paleo-redox conditions and constrain their tectonic affiliation based on the geochemical characteristics.

REGIONAL GEOLOGY

The Late Mesozoic to Early Cenozoic evolution of the Tethyan Ophiolite Belt is linked to the closure of the Tethyan Ocean and collision of the Indian and Eurasian Plates. These two tectonic events were marked by plate convergence, subduction of oceanic lithosphere, ophiolite obduction, high pressure-low temperature metamorphism and collision-accretion activities that altogether gave rise to Alpine-Himalayan and Burmese-Indonesian arc systems (Robertson, 2002; Acharyya, 2007; Aldanmaz et al., 2008; Saha et al., 2018;2019). In India, Cretaceous ophiolites have been recorded as parts of the Alpine-Himalayan and Indo-Burman orogenic belts. The NHO belt in the IMR represents a segment of Tethyan oceanic crust and upper mantle that was involved in an eastward convergence and collision of the Indian Plate with the Eurasian Plate at the Myanmar continental margin during the Late Cretaceous-Eocene (Ghose and Agarwal, 1989) (Figure 1a

inset). The Naga Hills with in the Ziphu Formation is a ~200 km long, ~5-10 km wide, westerly convex linear belt striking NE-SW (Table 1). It comprises of four major tectono-stratigraphic units, namely the Naga Metamorphic complex, the NHO suite, the Inner Fold belt and the belt of Schuppen (Ghose et al., 1987) (Table 1, Figure 1a). The Naga metamorphic complex, which is thrusted over the Upper Cretaceous–Eocene turbidite and NHO, marks the easternmost part of the belt. It is composed of the Saramati, Nimi, and Naga metamorphic. The Naga Metamorphic complex is made up of sheared granite, phyllite, limestone, marble, quartzo-feldspathic schist, and gneiss with minor serpentine (Table 1). The ophiolite belt of the Naga Hills, lies to the east of the Saramati Formation. It is composed of carbonaceous phyllites, quartz mica schist, and schistose quartzite. The clastic nature of the rocks, the graded bedding, and the cut-and-fill structures point to its sedimentary nature. The Naga ophiolitic complex strikes NNE-SSW for ~90 km and is tectonically sandwiched between the flyshoidal sediments of the Disang Formation to its western margin (Table 1) and overridden by the Nimi Formation of the Naga Metamorphic complex at its eastern margin (Kacker and Roy, 1980; Ghose et al., 2014) (Figure 1a). The Disang Formation consists of a folded sequence of slate, graphitic slate, phyllite, siltstone and fine-grained sandstone (Agrawal and Ghose 1986; Vidyadharan et al. 1989). The Nimi Formation, covering 18 × 12 km^2 area, is exposed at the eastern fringe of Nagaland. Non-crystalline limestone, quartzite, phyllite, carbonaceous phyllite, quartz sericite schist, and schistose granite are the main litho units of the Nimi Formation (Table 1).

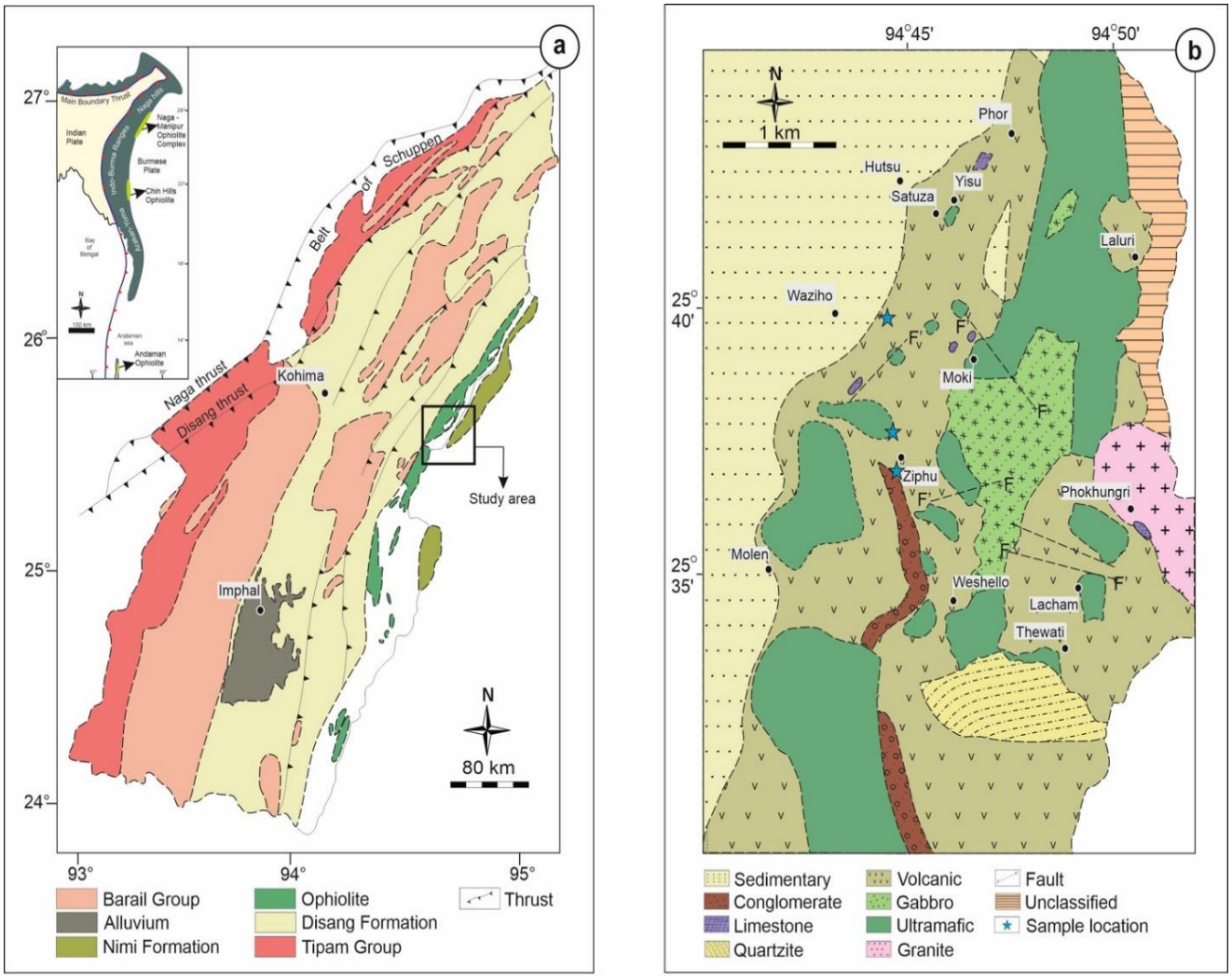

Figure 1. **(a)** Simplified geological and tectonic map of Nagaland and Manipur, India (modified after Geological Survey of India and Ningthoujam et al., 2012) inset: Simplified tectonic map of eastern margin of India depicting Naga-Manipur, Chin Hills and Andaman Ophiolitic complexes. **(b)** Geological map of Nagaland ophiolite with sample locations marked by star (modified after Agrawal and Ghose, 1986).

Table 1. Stratigraphy of Naga Hills, India (Modified after Mathur and Evans, 1964; DGM, 1978; Ghose et al., 2010, 2014)

Age	Group	Formation with lithology	
Oligocene	Barail	Jopi / Phokphur Formation Tuffaceous shale, sandstone, greywacke, gritand conglomerate. Minor limestone and carbonaceous matter	
Upper Cretaceous-Eocene	Disang	Upper	Flysch: Shale passing into slate alternating with sandstone. Presence of mega cross-bed, load cast, slumping structure and olistoliths. Evaporites.
		Lower	Flysch: Dominantly shale passing intoslate and phyllite (turbidite)
Middle Jurassic to Cretaceous	Ophiolite complex	Ziphu Formation Marine sediments (shale, phyllite, greywacke, iron-rich sediments, chert and limestone with radiolaria and coccoliths),volcanics (basalt, spilite,volcaniclastics), metabasics greenschist, glaucophane schist/glaucophane-bearing metachert, eclogite),layered cumulate sequence (peridotite, pyroxenite, gabbroids, plagiogranite), and peridotite tectonite and serpentinite associated with deposits of podiform chromite and nickeliferous magnetite, minor Cu-Mo sulphides associated with late felsic intrusions and some dolerite dykes	
		----Fault Thrust----	
Mesozoic (?)	Naga Metamorphic complex	Nimi Formation Weakly metamorphosed limestone, phyllite, quartzite and quartz-sericite schist	
		Naga Metamorphics Mica schist, granitoid gneiss and feldspathic metagreywacke with tectonic slices of ophiolite	

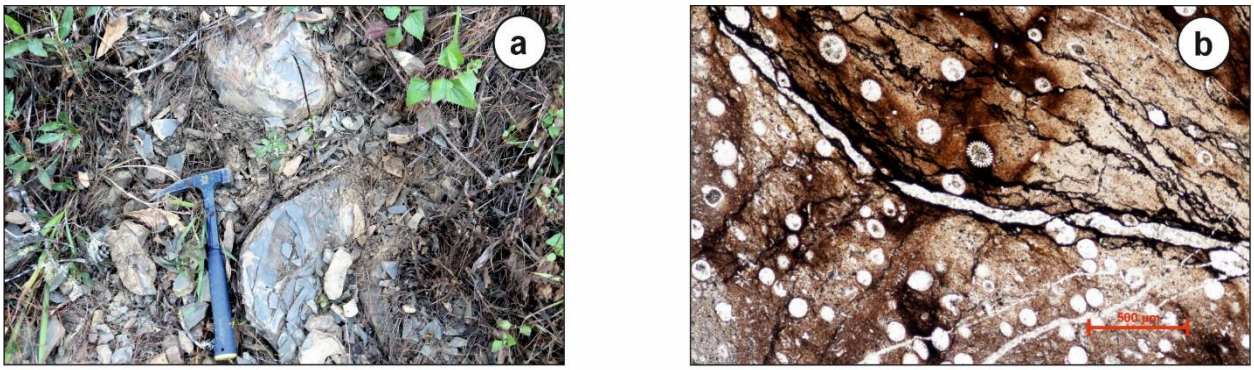

Figure 2. **(a)** Field photograph of an outcrop showing the occurrence of pelagic sediments. **(b)** Photomicrographs showing the presences of radiolarian microfossils in cherts from NHO.

FIELD GEOLOGICAL STUDIES

The NHO represents a thrusted assemblage dominated by mantle and crustal ultramafic-mafic lithologies (peridotites, dunites, pyroxenites, gabbros, olivine gabbros, norites, basalts) with minor felsic variants (plagiogranites) and pelagic sediments. The pelagic sediments include pelitic, calcareous and iron-rich sediments, and cherts. The pelitic sediments are represented by variegated shale, slate, phyllite and occasionally metamorphosed to schist. The sedimentary rocks include greywacke, arkose, subarkose and quartzite. The silica-rich cryptocrystalline cherts are extensively preserved among the marine sediments because of their resistance to weathering. They show a variety of colours including light grey, bluish grey, light green, dull to bright red and brown. They occur as thin beds and lenses interlayered with mafic volcanics.

In this study, fossiliferous red cherts occurring as beds and lenses intercalated with basalts were collected from in and around Waziho and Zipu area (Figure 1b and 2a). Previous study reported the presence of microfossils in cherts interlayered from the same areas. These include coccoliths, viz., *Zygolithus penticulus* and *Ahmullerella octoradiata*, and radiolarians, viz., *Cenozphaera* sp., *Spongodiscus* sp., etc., belonging to the Maastrichtian age (Agrawal, 1985); while radiolarian cherts from the northern sector of the NHO yielded a Late Jurassic age (Baxter et al., 2011) indicating sedimentation in the early Neotethys.

ANALYTICAL TECHNIQUES

A few selected samples from the study area were subjected to X-Ray diffraction analyses through XRD instrument Model: AXS D8 Advances (Make: Bruker Ltd Germany) at the CFC

(Common facility center)-SAIF (Sophisticated analytical instrumentation facility) Center; Shivaji University, Maharashtra. The slides were then analyzed in an X-ray diffractometer using Cu-Ka radiation source, acceleration voltage of 40 kV and tube current of 20 mA. The 2θ ranged from 5°–70°. The X-ray diffraction of the mineral were identified through respective D spacing values and intensity. The database used for mineral identification is webmineral.com.

Further, the seventeen samples were powdered a using tungsten carbide disc mill pulverizer at CSIR-National Institute of Oceanography, Goa. The powders were then analyzed for its major, trace and rare earth element concentrations along with geochemical reference materials for quality control. The concentration of major oxides was determined using X-ray fluorescence spectroscopy (XRF; PAN analytical™ Axios m AX4, microprocessor controlled, sequential XRF at CSIR-National Geophysical Research Institute, Hyderabad. In order to prepare the samples, ~ 2 gm of powdered samples were sprinkled onto a collapsible aluminum cup having a diameter of 4 cm initially filled with boric acid. Subsequently, these samples were compressed by applying a pressure of 25 tons using a hydraulic press (Hydraulic Press, Herzog, Germany). The analytical protocol used to carry out the procedures of pellet preparation was adopted from Krishna et al. (2007). Certified reference materials (CRMs) JA-1 (Japanese andesite, GSJ, Japan) and BHVO-1 (Hawaiian basalt, USGS, USA) were used as unknown samples to check the precision and reproducibility which were better than 5% RSD for all the major elements. The Loss on Ignition (LOI) was measured by taking 2 gm of sample in a quartz crucible and heating it in a muffle furnace upto ~900° C for 1 hour. The samples were then placed in a desiccator containing silica crystal. The reduction in weight measured after ignition was considered to be the loss of volatile content from the samples.

Trace elements, including rare earth elements (REE), were analyzed using a high-resolution inductively coupled mass spectrometer (HR-ICPMS). The preparation of the samples involved closed acid digestion of accurately measured 50 mg of each sample contained in Savillex® vials. This sample was treated by addition of a 7 mL mixture of supra pure HF and HNO_3 acids in 2:5 ratio into the Savillex® vials. The vials were placed on a hotplate and were heated for 72 hours at 110°C. After 72 hours, the caps were opened and the mixture was dried down and further treated with 1 mL of 2% HNO_3 until clear solution was obtained. The clear solution was once more evaporated and finally was diluted using 2% HNO_3 to prepare 50 mL stock solution for each sample along with procedural acid blank. The stock solution was further diluted 20,000 times for analyses in high resolution inductively coupled mass spectrometer (HR-ICP-MS) (Nu Instruments™ Attom, UK) at CSIR-National Institute of Oceanography, Goa. ^{103}Rh was used as an internal standard. CRMs namely, JA-1 and JB-2 (Geological Survey of Japan, Japan) were used as unknown quality standards to assess the accuracy and precision of the obtained data. For most of the elements, the accuracy and precision of the obtained data were within 10% RSD . (Please see Appendix 1)

RESULTS

Petrography and mineralogy

Seventeen samples of cherts were collected in the field. Representative samples were polished to prepare thin sections, which were studied under reflected and transmitted light using Nikon eclipse LV100 POL optical microscope at CSIR-National Institute of Oceanography (NIO), Goa, India. Petrographic studies of the cherts from NHO show the presence of dominantly quartz, with recrystallized secondary quartz veins along with minor amount of carbonate minerals. Uneven spongy (or honeycombed) interior fabrics are frequently seen in well-preserved silica mounds, with localized interconnecting channels and veins. There were several vesicles or cavities inside the mounds, but they were primarily blocked by radiating micro-quartz and fibrous recrystallized silica. Abundant microfossils of radiolarian tests are preserved within the chert (Figure 2b). X-Ray diffraction (XRD) study confirm the presence of silica as major constituent within the chert. XRD studies for most of the samples reveal prominent peaks of quartz (Figure. 3).

Whole rock geochemistry

The bulk chemical composition of NHO cherts is dominantly characterized by high SiO_2 content from 71.17 to 79.32 wt. %, moderate $Fe_2O_3^{(t)}$ and CaO ranging from 4.47 to 5.98 wt. % and 6.9 to 7.14 wt. % respectively; restricted Al_2O_3 and MgO concentrations ranging from 2.47 to 4.33 wt. and 2.25 to 2.72 wt.% respectively. The total alkali content ranges from 2.08-3.43 wt. %, MnO contents range from 0.30 to 0.90 wt. % and TiO_2 concentrations ranges from 0.12 to 0.27 wt. %. The Loss on Ignition (LOI) ranges from 1.19 to 2.85 wt. %. The major oxide analyses are provided in Table 2.

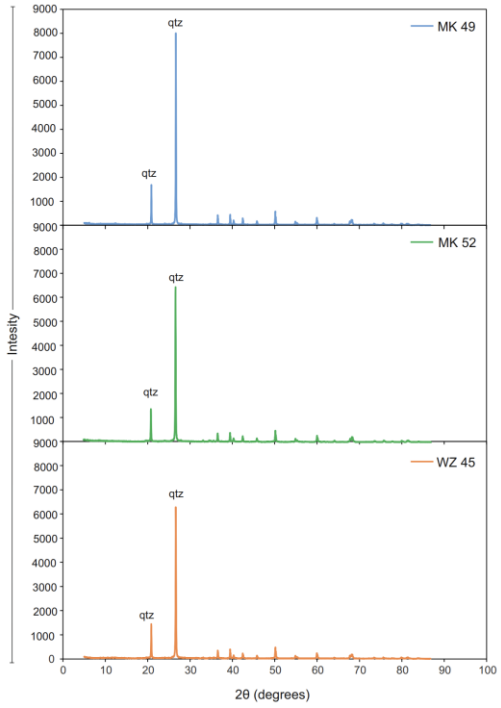

Figure 3. X-ray diffraction (XRD) patterns for the studied chert samples.

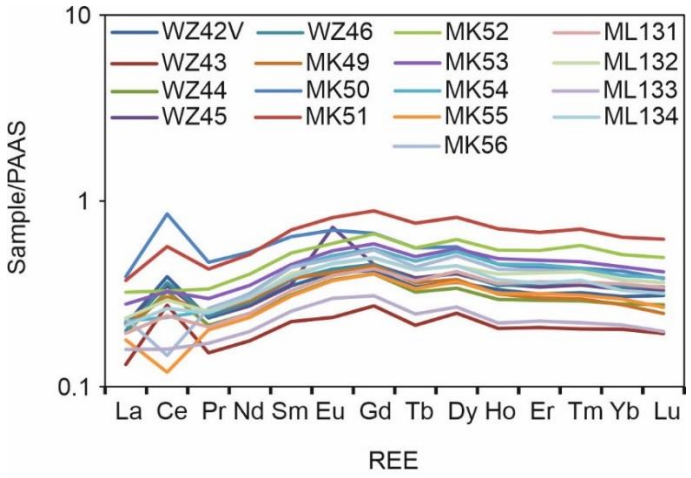

Figure 4. PAAS normalized REE patterns for the collected chert samples from NHO. Normalizing factors are from Taylor and McLennan (1985)

The studied cherts are marked by a wide variation and relatively higher concentration of transition metals like Co and Ni with Co ranging from 76.80 to 169.80 ppm (avg. 120.62 ppm; except ML134 Co: 1.25); and Ni spanning from 14.55 to 104.58 ppm (avg. 31.37ppm) as compared to Upper crust (UCC; Co: 10 ppm, Ni: 20 ppm; Taylor and McLennan, 1995) (Table 2). The average Cr concentration (15.61 ppm) is however lower as compared to UCC composition (35 ppm; Taylor and McLennan, 1995). The studied chert samples from NHO have ΣREE (32.82-117.72 ppm), lower than both the NASC (North American Shale Composite:172 ppm, and PAAS (Post Archean Australian shale:183 ppm, Taylor and Mclenan, 1985) (Table 2). The PAAS normalized REE profile depicts a convex upward pattern (Figure 4). This observation is further substantiated in the PAAS normalized REE ratios of $(La/Sm)_N$ ranging from 0.51 to 0.63 (avg.0.58), $(Gd/Yb)_N$ ranging from 1.21 to 1.62 (avg.1.40) and $(La/Yb)_N$ ranging from 0.54 to 0.93 (avg. 0.66) (Table 2). The PAAS normalized REE patterns also display a positive anomaly for Ce and negative anomalies for Eu and Tb (Figure 4). The Ce/Ce* ranges from 0.59 to 1.98 (avg. 1.34) and Eu/Eu* ranges from 0.33 to 0.80 (avg. 0.50) for the studied chert samples from NHO (Table 2)

Table 2. Major oxides and trace elements of chert samples collected from NHO

Sample ID	WZ42V	WZ43	WZ44	WZ45	WZ-46	MK49	MK50	MK51	MK52
(wt.%)									
SiO_2	77.91	76.67	75.92	76.83	76.57	76.54	75.56	71.17	75.97
Al_2O_3	2.62	3.96	3.84	2.76	2.80	2.82	3.21	4.33	2.89
$Fe_2O_3^{(t)}$	4.87	4.64	4.77	4.87	4.89	4.86	5.20	5.98	5.16
MnO	0.29	0.31	0.26	0.30	0.21	0.62	0.90	0.56	0.36
MgO	2.33	2.37	2.46	2.39	2.37	2.43	2.61	2.72	2.38
CaO	7.08	6.92	6.99	7.08	7.07	6.96	6.90	7.00	7.07
Na_2O	1.78	1.66	1.77	1.82	1.87	1.55	1.41	1.74	1.78
K_2O	0.86	0.60	0.87	0.89	1.07	0.79	0.79	1.68	1.17
TiO_2	0.16	0.13	0.16	0.17	0.17	0.14	0.15	0.27	0.18
P_2O_5	0.01	0.02	0.01	0.02	0.02	0.01	0.05	0.02	0.01
LOI	1.49	1.37	1.51	1.69	1.55	1.61	2.21	2.85	1.66
Sum	99.4	98.7	98.6	98.8	98.6	98.3	99.0	98.3	98.6

Sample ID	WZ42V	WZ43	WZ44	WZ45	WZ-46	MK49	MK50	MK51	MK52
(ppm)									
Cr	12.25	9.58	12.60	13.43	13.13	11.10	16.36	18.98	12.36
Co	170	145	120	152	97.60	99.46	169.2	76.80	87.40
Ni	16.66	20.21	14.55	16.80	24.96	39.55	104.58	51.73	35.83
Rb	16.73	11.83	17.67	18.26	20.80	13.41	16.57	41.89	24.16
Sr	23.30	19.07	24.93	60.44	26.44	18.17	25.28	29.88	23.24
Cs	0.62	0.40	0.70	0.66	0.84	0.31	0.41	1.62	0.76
Ba	167.5	121.9	522.6	5680	310.4	56.25	63.58	121.13	82.57
Sc	4.48	3.00	3.62	4.00	5.04	3.07	4.10	8.17	4.83
V	14.61	10.70	10.62	12.81	10.82	17.44	29.62	35.55	20.87
Ta	0.03	0.00	0.02	0.02	0.02	0.01	0.00	0.02	0.02
Nb	0.38	0.03	0.25	0.13	0.20	0.08	0.06	0.33	0.24
Zr	16.71	8.25	15.86	16.50	22.14	12.58	15.62	41.03	22.24
Hf	0.50	0.26	0.46	0.45	0.62	0.36	0.41	1.15	0.63
Th	1.79	0.88	1.81	1.74	2.64	1.03	1.24	3.03	1.59
U	0.82	0.68	0.29	0.30	0.33	0.37	0.35	0.44	0.26
Y	10.37	6.27	10.32	12.30	11.52	9.60	13.33	21.66	18.02
Li	15.42	16.06	16.80	17.49	19.03	11.09	16.65	9.77	11.18
La	8.19	5.00	7.42	8.33	7.61	8.20	14.88	14.18	12.27
Ce	31.35	22.00	26.11	27.94	28.99	24.38	68.09	45.53	26.18
Pr	2.09	1.35	1.91	2.13	2.14	2.24	4.15	3.83	2.99
Nd	8.71	5.66	7.92	8.75	9.07	9.35	16.94	16.48	12.94
Sm	1.95	1.26	1.75	1.99	2.11	2.15	3.59	3.91	2.94
Eu	0.45	0.26	0.41	0.79	0.47	0.45	0.77	0.89	0.65
Gd	1.98	1.28	1.90	2.14	2.14	2.10	3.15	4.16	3.13
Tb	0.27	0.17	0.25	0.30	0.29	0.28	0.43	0.58	0.43
Dy	1.61	1.09	1.49	1.79	1.82	1.66	2.49	3.59	2.72
Ho	0.33	0.21	0.30	0.36	0.35	0.32	0.46	0.71	0.54
Er	0.91	0.60	0.85	1.00	1.04	0.87	1.27	1.96	1.57
Tm	0.13	0.08	0.12	0.14	0.15	0.12	0.17	0.28	0.23
Yb	0.86	0.57	0.78	0.94	0.97	0.77	1.17	1.79	1.44
Lu	0.13	0.08	0.12	0.14	0.15	0.11	0.16	0.27	0.21
∑REE	124.1	85.7	111.4	122.5	129.7	108.6	199.1	219.3	148.1
Cu	27.22	35.69	20.01	33.14	37.52	103.2	101.1	31.97	33.09
Zn	0.00	0.00	0.00	0.00	0.00	0.00	5.54	0.00	-
Ga	16.08	12.20	43.09	484.32	28.19	7.33	8.75	15.47	9.84

Table 2 (Contd….)

Sample ID	MK53	MK54	MK55	MK56	ML131	ML132	ML133	ML134
(wt.%)								
SiO_2	75.59	77.46	76.93	75.50	76.46	77.56	78.41	79.32
Al_2O_3	2.94	2.66	2.75	2.96	2.92	2.66	2.60	2.47
$Fe_2O_3^{(t)}$	5.23	4.97	4.67	4.95	5.78	5.01	4.47	4.81
MnO	0.36	0.27	0.03	0.05	0.25	0.30	0.58	0.49
MgO	2.38	2.33	2.45	2.58	2.32	2.30	2.38	2.25
CaO	6.96	6.99	7.04	7.08	7.12	7.14	6.92	6.96
Na_2O	1.67	1.70	2.11	2.24	1.90	2.06	1.71	1.71
K_2O	1.40	1.12	0.80	1.07	0.79	1.05	0.37	0.64
TiO_2	0.19	0.16	0.15	0.18	0.15	0.17	0.12	0.15
P_2O_5	0.03	0.02	0.03	0.03	0.01	0.03	0.02	0.03
LOI	1.79	1.76	1.51	2.04	1.19	1.42	1.35	1.69
Sum	98.5	99.4	98.5	98.7	98.9	99.7	98.9	100.5

Sample ID	MK53	MK54	MK55	MK56	ML131	ML132	ML133	ML134
(ppm)								
Cr	12.52	12.86	35.93	48.83	13.06	14.56	7.32	0.51
Co	100	139	146	138	135	124	149	1.25
Ni	37.82	29.99	26.78	35.11	23.02	26.83	28.38	0.49
Rb	27.82	22.73	15.97	21.93	16.56	20.23	7.50	13.17
Sr	20.34	18.97	23.73	28.64	23.33	24.94	22.04	27.01
Cs	0.83	0.65	1.21	1.64	0.57	0.67	0.30	0.54
Ba	129	96.09	133.2	156.5	35.49	40.43	52.35	69.32
Sc	5.18	3.97	4.38	5.89	4.14	4.83	2.63	3.82
V	25.01	19.28	22.65	28.39	14.99	16.00	8.76	0.20
Ta	0.02	0.01	-0.01	0.00	0.02	0.01	0.00	0.00
Nb	0.16	0.17	0.03	0.08	0.26	0.20	0.05	0.11
Zr	22.22	14.75	13.82	22.89	13.59	19.57	8.92	14.71
Hf	0.64	0.40	0.43	0.64	0.36	0.54	0.25	0.43
Th	1.76	1.17	0.84	1.21	1.17	1.60	0.58	1.07
U	0.29	0.22	0.62	0.45	0.20	0.23	0.90	0.79
Y	16.08	15.22	11.82	15.25	12.65	13.66	6.96	11.77
Li	9.74	8.87	9.20	10.53	9.92	9.85	31.98	21.32
La	10.57	8.57	6.79	8.86	7.37	8.88	6.03	8.12
Ce	26.04	18.86	9.58	11.78	19.29	23.47	12.76	21.09
Pr	2.66	2.29	1.80	2.35	1.86	2.26	1.53	2.22
Nd	11.22	10.17	7.55	10.04	7.95	9.65	6.34	9.71
Sm	2.55	2.46	1.72	2.45	1.84	2.27	1.43	2.18
Eu	0.59	0.56	0.41	0.54	0.44	0.50	0.33	0.51
Gd	2.76	2.60	1.90	2.56	2.03	2.31	1.45	2.33
Tb	0.39	0.36	0.26	0.34	0.29	0.33	0.19	0.33
Dy	2.43	2.35	1.62	2.23	1.83	1.96	1.18	1.97
Ho	0.49	0.46	0.32	0.43	0.36	0.40	0.22	0.38
Er	1.39	1.31	0.92	1.24	1.07	1.19	0.65	1.05
Tm	0.19	0.17	0.12	0.17	0.15	0.17	0.09	0.15
Yb	1.24	1.11	0.83	1.05	1.00	1.06	0.60	0.92
Lu	0.18	0.17	0.11	0.16	0.15	0.16	0.09	0.14
∑REE	143.8	115.5	97.73	129.51	102.9	121.1	93.9	105.3
Cu	26.19	23.87	38.69	40.08	81.18	88.77	31.19	0.01
Zn	-	-	-	-	-	-	-	0.50
Ga	13.80	10.10	13.41	16.41	5.20	6.10	6.14	7.63

DISCUSSION

Depositional environments

Input from major elements

The primary source for silica is either terrigenous, biogenic i.e. from the siliceous tests and spicules of radiolarians and sponges or chemically precipitated from hydrothermal solutions (Adachi et al., 1986). Fe_2O_3 is relatively enriched in sediments near mid-oceanic ridges and accordingly, has been employed as an indicator of hydrothermal activities. The low TiO_2/Al_2O_3 values ranging from 0.03 to 0.06 (avg.0.06) and higher Fe_2O_3/Al_2O_3 ranging from 1.17 to 1.98 (avg. 1.70), in conjunction with low Cr concentration (avg. 15.61 ppm) in comparison to PAAS (Cr: 110 ppm), negates detrital origin of these cherts and lowers the potential of its source from continental margin environments (Thong et al., 2022). Majority of the samples also exhibit high MnO/TiO_2 values (>1, avg. 2.28) indicative of metalliferous input (Adachi et al., 1986). The studies of Bostrom and Peterson (1969) suggested that the proportion of Al/(AI+Fe+Mn) in marine sediments, serves as an indicator of the hydrothermal influence on sediment composition. In this study, the Al/(AI+Fe+Mn) ratio ranges from 0.26 to 0.38 (avg. 0.30), which is comparably intermediate between the values of hydrothermal cherts (0.01) and biogenic hemiplegic cherts (0.60) from East Pacific rise. However, in the Al-Fe-Mn ternary diagram, the samples of NHO cherts plot within the hydrothermal field (Figure 5a). The $Al_2O_3/(Al_2O_3+Fe_2O_3)$ ratio for most of the studied cherts, varies from 0.34-0.46, which is lower than those of cherts from pelagic basins (<0.4) and continental margins (0.5-0.9) but almost in the range of cherts proximal to mid oceanic ridge (0.4-0.7).

Input from trace elements

In terms of trace elements, U and Th are considered noteworthy elements in distinguishing the hydrothermal and non-hydrothermal origin of sediments (Owen et al., 1999). Normal seawater is generally considered to be enriched in Th, contrastingly hydrothermal water is enriched in U. Therefore, in a non-hydrothermal environment the value of U/Th is less than 1. The U/Th ratio of NHO cherts is less than 1 (0.12–0.78, expect sample ML133 U/Th: 1.57), which is indicative of a normal biogenic sediment with little hydrothermal influence. The PAAS normalized REE patterns however reflect positive Ce anomaly and relatively enriched HREEs which are akin to hydrothermal cherts (Murray, 1994) (Figure 4). Apart from this, The Y/Ho ratio noted for the studied chert samples from NHO to be slightly fractionated ranging from 29.17 to 37.30 similar to chondritic values (28.75; Sun and McDonough, 1989) rather than supra chondritic values resulting from higher residence time of Y as compared to Ho in seawater (Girty et al., 1996; Nozaki et al.,1997) common to hydrothermal waters. The abundance of radiolarian tests seen in petrographic thin sections (Figure. 2b) likely suggests the origin of these cherts to be biogenic as well hydrothermal in origin, which are akin to hydrothermal cherts as observed in previous studies of Adachi et al., (1986).

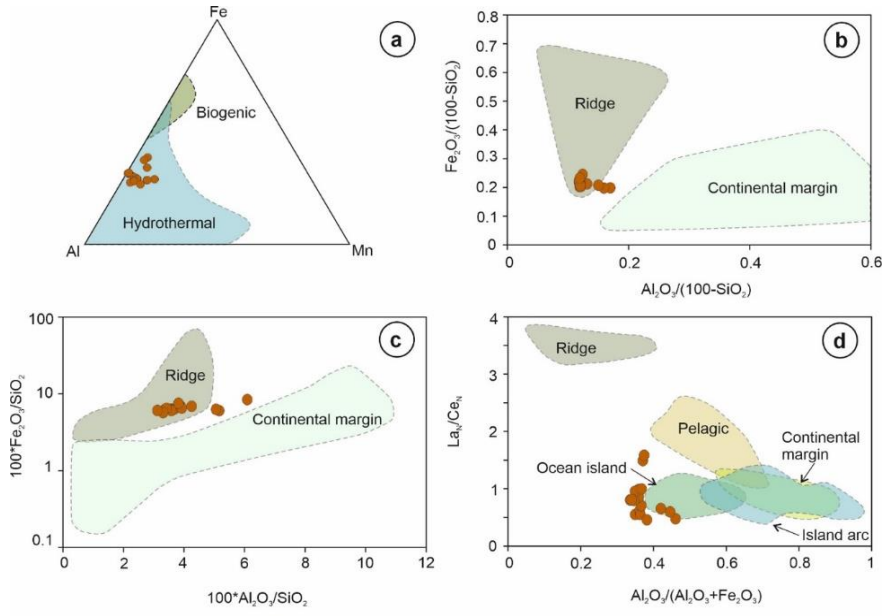

Figure 5. **(a)** Ternary plots of Al-Fe-Mn exhibiting hydrothermal source for the NHO chert (after Bostrom and Peterson, 1969; Yamamoto, 1983; Adachi et al., 1986). Plots showing **(b)** $Al_2O_3/(100-SiO_2)$ vs. $Fe_2O_3/(100-SiO_2)$ after Murray, (1994), **(c)** $100*(Al_2O_3/SiO_2)$ vs. $100*(Fe_2O_3/SiO_2)$ after Murray (1994), and **(d)** $(La/Ce)_N$ vs. $Al_2O_3/(Al_2O_3+SiO_2)$ after Girty et al. (1996) and Murray (1994)tectonic discrimination for the studied cherts.

The REE chemistry is an important indicator to delineate the connection between distinct components in marine system due to their higher susceptibility during post-burial diagenesis (Murray et al., 1990). The REE content in cherts is influenced by terrigenous input, metalliferous materials in hydrothermal fluids from mid-ocean ridges, and the rate of REE absorption. The total REE concentration (ΣREE) trend increases from minimum values of around 10.9 ppm in a mid-oceanic ridge environment to up to 400-500 ppm [6] passing away from the ridge in an ocean basin setting, with values being highly scattered, but declining for a continental margin setting (4-110 $\times 10^{-6}$; Murray et al., 1990). The studied chert samples from NHO have ΣREE (32.82-117.72 ppm) lower than PAAS. Studies of Murray et al. (1990) and Murray (1994) are suggestive that cherts formed in close vicinity of ocean ridge environment have La_N/Ce_N ratio greater than 3.5 while a ratio of approximately 1 is indicative of proximity to continental margins. Cherts from the NHO have a positive correlation with Al_2O_3 and TiO_2 and the La_n/Ce_n and Ce/Ce* ratios have a negative correlation, indicating that REE is primarily determined by the influence of terrigenous source. The Ce anomalies are extremely low at the mid-oceanic ridge (Ce/Ce*~0.29), slightly higher in ocean basins (Ce/Ce*~0.55) and increases at continental margins (Ce/Ce*~0.90 to 1.30). The Ce/Ce* is greater than 1 for majority of the studied samples underpinning the influence of the terrigenous source. Rb and Th in the cherts are mainly sourced from continental provenances and are difficult to dissolve in sea water. The positive correlation of Rb, and Th contents with TiO_2, reflects the influx of terrigenous sources. Additionally the diagram showing $(La/Ce)_N$ vs $Al_2O_3/(AL_2O_3+Fe_2O_3)$ indicate they were deposited in pelagic to ocean island environment (Murray, 1994; Girty et al., 1996) (Figure 5d).

The U/Th, Ni/Co and V/(V+Ni) record paleo-redox conditions in the environment of deposition. The U/Th values of <0.75, 0.75-1.25 and >1.25 represent oxic, dysoxix and anoxic redox conditions respectively (Kiliç et al., 2018). The Ni/Co value of <5 are suggestive of oxic depositional states, 5< Ni/Co< 7 values represent dysoxic states and >7 are suggestive of anoxic depositional states (Jonnes and Manning, 1994). In the case of V/V(V+Ni), oxic, dysoxic and anoxic environments are characterized by values ranging <0.46, 0.40-0.60 and 0.54-0.82 respectively (Hatch and Levanthal, 1992). The studied cherts from NHO are corroborating oxic paleo-redox environments as collectively reflected from the values of U/Th ranging from 0.12-0.74 (except for 2 samples); Ni/Co ranging from 0.10-0.67 and V/V(V+Ni) ranging from 0.22-0.47. Additionally, Deng et al. (2017) stated that exceptionally low U are indicative of an oxic deposition. The studied cherts have very low U concentrations 0.20-0.90 ppm which is in accordance with this study.

Geodynamic setting

Field observations and geochemical attributes ubiquitously contribute to comprehend the geodynamic conditions that facilitated the deposition of NHO cherts. These cherts with radiolarian assemblage are oceanic sediments overlying the ultramafic-mafic sequence of NHO and are found interlayered with the ophiolitic basalts. This indicates that the deposition of these cherts post-dated the formation of NHO ultramafic-mafic crust-mantle assemblage and is contemporaneous with basalt volcanism. Thong et al. (2022) suggested that the cherts were deposited in an open ocean basin distal from ridge axes, followed by non-hydrothermal sedimentation under oxic conditions. Micropaleontological and geochemical studies infer that the red cherts of NHO were formed in Upper Jurassic in an active continental margin settings (Ayyamperumal et al., 2021; Aitchison et al., 2019; Baxter et al., 2011). Verencar et al. (2022; 2024a,b) envisaged a SSZ setting marked by subduction initiation, fore-arc extension, subsequent mantle wedge metasomatism and melting for the generation of the ultramafic mafic plutonic lithologies comprising the crust and restitic mantle section of NHO. Previous workers have deduced diverse tectonic environments for the formation of the volcanic sequence of NHO. The basalts of NHO have been classified as Low Ti and High Ti basalts by Sengupta et al. (1989) and Rao et al. (2010). The low Ti rocks were attributed to have overlapping geochemical signatures of MORB and island arc, where as, high Ti basalts have been associated with ocean island volcanism. The distinct hydrothermal and terrigenous signatures for the NHO cherts, as reflected by their geochemical features, conspicuously invoke an expansive depositional realm between a ridge proximal set up and active continental margin aligning with the duality in signature observed for most basalts of the NHO. The geochemical characteristics of the cherts from NHO, clearly indicate spatial variability in their formation from near mid-oceanic ridge to close to continents. Al_2O_3, TiO_2, ΣREE, Ce/Ce*, $(La/Ce)_N$ and other geochemical proxies along with the radiolarian assemblages altogether, suggest a hydrothermally controlled deposition near the mid oceanic ridge with the influence of terrigenous input. Further, the presence of silica cements in voids and channels were not a consequence of silica replenishment; rather, they were a byproduct of interactions between sea water and hydrothermal fluids that caused the silica-rich fluid to rapidly cool. The growth of this silica is influenced by fluid pH levels (Heaney, 1993; Wang et al., 2012). This is preferred in acidic siliceous solutions that cool quickly because silica polymer cross-branching is widely suppressed (Hopkinson et al., 1999; Wang et al., 2012). Recent studies by Imtisunep et al. (2022) suggests a duality in geochemical characters of basalts i.e. N-MORB and E-MORB (enriched-MORB) character. It has been indicated that in general, underlying pillow lavas are showing depleted N-MORB type characters with almost flat LREE patterns

although some amount of E-MORB with enriched REE patterns and depleted HFSE concentrations are also reported from the studied area.

The MORB, IAT and OIB signatures for the basalts associated with the cherts, could be inferred to be linked with waning stage of subduction involving (i) metasomatism and partial melting of mantle wedge generating arc basalts and (ii) arc-rifting in response to slab-pull and subduction retreat thereby stimulating MORB and OIB melt generation though decompression melting of upwelling asthenosphere. Normal faults generated during arc rifting serve as pathways for extensive hydrothermal activity further aided by magma upwelling providing the heat source for seawater circulation. The hydrothermal components for NHO cherts are thus interpreted to be sourced from arc-rifting during subduction termination and ocean basin closure, while the terrigenous input could be derived from the continental margin. Thus, the NHO cherts were deposited in a rifted arc basin, generated by pronounced hydrothermal activity and terrigenous contributed from active continental margin. The major oxide of the studied chert samples are also indicative of a ridge proximal source (Figure 5b, c).

Ocean basins associated with diverse tectonic realms including abyssal ocean basin, back-arc basin, island arc, continental rift basin are envisaged as favorable environments for deposition of cherts. This distinct tectonic affiliation is imprinted on the lithological features and geochemical attributes of the deposited cherts. Major and trace element geochemistry of Middle Jurassic radiolarian cherts, associated with Dajiweng ophiolite of SW Tibet, conform to a transitional environment between an ocean basin and active continental margin (Cui et al., 2021). Likewise, the geochemical features of ophiolitic cherts from Qinling orogenic belt suggest their deposition in an extensional ocean basin closely associated with an active continental margin (Zhang et al., 2004). REE signatures of Arenig cherts from Ballantrae ophiolite, southern Scotland, propound their formation in a rifted arc basin close to an active continental margin. (Armstrong et al,1999).

The Tethyan ophiolites viz. Pindos ophiolite (Greece), Kizildag ophiolites (Turkey), Troodos ophiolites (Cyprus) and Semail ophiolites (Oman), hosts Fe-Cu ore deposits, metalliferous sedimentary rocks, red and Mn-rich cherts evidencing hydrothermal activity (Gills and Banerjee, 2000). Though the studies of Thong et al. (2022) support that the silica of these Late Jurassic-Early Cretaceous NHO cherts are, pre-dominantly biogenic and are derived from radiolarians and other siliceous microfossils in an open ocean basin, distal from oceanic ridge axes, however; few samples also show identical ocean island characteristics and minor signatures of influence of hydrothermal solutions. The bio stratigraphic correlations indicate a wide geological time from Neo-Tethyan basin opening to nearing closure i.e. Late Jurassic to Late Cretaceous (Agrawal, 1985; Baxter et al., 2011). The bimodal contribution of terrigenous and hydrothermal components towards the deposition of NHO cherts corroborates a rifted arc basin, in close association with active continental margin set up. This transitional tectonic regime complies with magmatism and subsequent sedimentation in a rifted arc basin proximal to an active continental margin tectonically concomitant to slab tearing and subduction termination, ocean basin closure and consequent accretion-collisional processes.

CONCLUSION

This study demonstrates the origin and depositional environment of cherts from NHO in terms of its geochemical characteristics. Following main conclusions are drawn from this study:

(i) Geochemical data suggest a hydrothermal origin for the studied cherts along with input from the terrigenous source.

(ii) Occurrence of radiolarian tests are indicative of presence of biogenic silica.

(iii) The paleo-redox conditions demonstrated by U/Th, V/(V+Ni), Ni/Co values for the studied chert samples, corroborate an oxic environment for their deposition.

(iv) This study infers a transitional tectonic realm associated with magmatism and subsequent sedimentation in a rifted arc basin proximal to an active continental margin.

Acknowledgements:

AV and AS are grateful to the Director, CSIR-National Institute of Oceanography for his encouragement, support and permission to publish this work. AS acknowledges the funding received from the Science and Engineering Research Board (SERB), Govt. of India under ECR/2018/000309. The authors sincerely acknowledge Mr. Robin John, Central Analytical Facility, CSIR-NIO for his kind help during HR-ICPMS data generation. The authors sincerely acknowledge the facilities received from the CFC (Common facility center)-SAIF (Sophisticated analytical instrumentation facility) Center; Shivaji University Shivaji University for XRD analyses. AV acknowledges Council of Scientific and Industrial Research (CSIR) for Senior Research Fellowship (Grant no. RF85094) and Goa State Research Foundation (GSRF) for necessary funding. We also thank two anonymous reviewers and Editor-in-chief for their constructive comment and suggestions. This is part of Ph.D. thesis of AV. This is NIO's contribution no.7388.

Author Credit Statement

AV: Investigation, visualization and writing-original draft, AS: Conceptualization; visualization data curation; funding

acquisition; methodology; project administration, supervision, writing-review and editing, RM: Formal analysis, writing-review and editing.

Data Availability

Data can be made available on reasonable request to the corresponding author

Compliance with Ethical Standards

The authors declare that they have no conflict of interest and adhere to copyright norms.

References

Acharyya, S. K., 2007. Collisional emplacement history of the Naga-Andaman ophiolites and the position of the eastern Indian suture. J. Asian Earth Sci., 29, 229-242.

Adachi, M., Yamamoto, K. and Sugisaki, R., 1986. Hydrothermal chert and associated siliceous rocks from the northern Pacific their geological significance as indication of ocean ridge activity. Sediment. Geol., 47, 125-148.

Agrawal, O. P. and Ghose, N. C., 1986. Geology and stratigraphy of the Naga Hills ophiolite between Melluri and Awankhoo, Pheek District, Nagaland, India. In Indian chapter IGCP Projects 195 and 197. Meeting (pp. 163-195).

Agrawal, O. P., 1985. Geology and geochemistry of the mafic-ultramafic complex of Indo-Burman ranges between Meluri and Awankhoo, Phek district, Nagaland, India. Unpublished Ph. D. thesis, Patna University, Patna.

Aitchison, J. C., Ao, A., Bhowmik, S., Clarke, G. L., Ireland, T. R., Kachovich, S., Lokho, K., Stojanovic, D., Roedae, T., Truscott, N., Zhen Y. and Zhou, R., 2019. Tectonic evolution of the western margin of the Burma microplate based on new fossil and radiometric age constraints. Tectonics, 38, 1718-1741.

Aldanmaz, E., Yaliniz, M. K., Guectekin, A. Y. K. U. T. and Göncüoğlu, M. C., 2008. Geochemical characteristics of mafic lavas from the Neotethyan ophiolites in western Turkey: implications for heterogeneous source contribution during variable stages of ocean crust generation. Geol. Magazine, 145, 37-54.

Ao, A., and Bhowmik S. K., 2014. Cold subduction of the Neotethys: the metamorphic record from finely banded lawsonite and epidote blueschists and associated metabasalts of the Nagaland Ophiolite Complex, India. J. Metamorphic Geol., 32, 829-860.

Armstrong, H. A., Owen, A. W. and Floyd, J. D., 1999. Rare earth geochemistry of Arenig cherts from the Ballantrae Ophiolite and Leadhills Imbricate Zone, southern Scotland: implications for origin and significance to the Caledonian Orogeny. J. of the Geol. Soc., 156, 549-560.

Ayyamperumal, R., Sooriamuthu, R., Gopalakrishnan, G., Biswa, G., Perumal, R., Gahlaut, P., Nuzrat, N. and Antony, J. K., 2021. Micropalaeontological and Geochemical Evidence of the Late Jurassic Radiolarians Cherts of Naga Ophiolite Hill, Nagaland, Northeast-India. Open J. Geology, 11, 356-372.

Baxter, A. T., Aitchison, J. C., Zyabrev, S. V. and Ali, J. R., 2011. Upper Jurassic radiolarians from the Naga ophiolite, Nagaland, northeast India. Gond. Res., 20, 638-644.

Bhowmik, S. K., and Pradhan, B., 2024. Mesozoic tectonics of the Indo-Burmese wedge: a record from the high-pressure metamorphic rocks of the Nagaland-Manipur Ophiolite Belt, NE India. Proc. Indian National Science Academy, 1-13.

Bhowmik, S. K., Ao, A., and Rajkakati, M., 2022. Tectonic framework of the high-pressure metamorphic rocks of the Nagaland Ophiolite Complex, North-east India, and its geodynamic significance: A review. Geol. J., 57, 727-748.

Bostrom, K. and Peterson, M. N. A., 1969. The origin of aluminum poor ferromanganoan sediments in areas of high heat flow on the East Pacific Rise. Marine Geol., 7, 427–447.

Chatterjee, N., and Ghose, N. C., 2010. Metamorphic evolution of the Naga Hills eclogite and blueschist, Northeast India: implications for early subduction of the Indian plate under the Burma microplate. J. Metamorphic Geol., 28, 209-225.

Cui, X., Luo, H., Aitchison, J. C. and Li, X., 2021. Middle Jurassic radiolarians and chert geochemistry, Dajiweng ophiolite, SW Tibet: Implications for Neotethyan Ocean evolution. J. Asian Earth Sci., 221, 104947

Deng, Y., Ren, J., Guo, Q., Cao, J., Wang, H. and Liu, C., 2017. Rare earth element geochemistry characteristics of seawater and porewater from deep sea in western Pacific. Scientific Reports, 7, 16539.

Dey, A., Hussain, M. F. and Barman, M. N., 2018. Geochemical characteristics of mafic and ultramafic rocks from the Naga Hills Ophiolite, India: implications for petrogenesis. Geosci. Frontiers, 9, 517-529.

DGM, 1978. Directorate of Geology and Mining, Nagaland, Misc. Publ. No. 1,1978.

Garbán, G., Martínez, M., Márquez, G., Rey, O., Escobar, M., and Esquinas, N., 2017. Geochemical signatures of bedded cherts of the upper La Luna Formation in Táchira State, western Venezuela: Assessing material provenance and paleodepositional setting. Sediment. Geol., 347,130–147

Ghose, N. C. and Agrawal, O. P., 1989. Geological framework of the central part of Naga Hills. Phanerozoic ophiolites of India and associated mineral resources. Sumna Publications, Patna, 165-188.

Ghose, N. C., Agrawal, O. P. and Srivastava, S. C., 1987. Metamorphism of the ophiolite belt of Nagaland, NE India. In: Proc. National Seminar Tertiary Orogeny, pp. 189-213.

Ghose, N. C., Agrawal, O. P., and Chatterjee, N., 2010. Geological and mineralogical study of eclogite and glaucophane schists in the Naga Hills Ophiolite, Northeast India. Island Arc, 19, 336-356.

Ghose, N. C., Chatterjee, N. and Fareeduddin, A., 2014. A petrographic atlas of ophiolite: an example from the Eastern India-Asia collision zone (p. 216). Springer India.

Gillis, K. M. and Banerjee, N. R., 2000. Hydrothermal alteration patterns in supra-subduction zone ophiolites. Special Papers-Geological Society of America, 283-298.

Girty, G. H., Ridge, D. L., Knaack, C., Johnson, D. and Al-Riyami, R. K., 1996. Provenance and depositional setting of Paleozoic chert and argillite, Sierra Nevada, California. J. Sediment. Res., 66, 107–118.

Hatch, J. R., and Leventhal, J. S., 1992. Relationship between inferred redox potential of the depositional environment and geochemistry of the Upper Pennsylvanian (Missourian) Stark Shale Member of the Dennis Limestone, Wabaunsee County, Kansas, USA. Chem. Geol., 99, 65-82.

Heaney, P. J., 1993. A proposed mechanism for the growth of chalcedony. Contr. Mineralogy and Petrology, 115, 66-74.

Hopkinson, L., Roberts, S., Herrington, R. and Wilkinson, J., 1999. The nature of crystalline silica from the TAG submarine hydrothermal mound, 26 N Mid Atlantic Ridge. Contr. Mineralogy and Petrology 137, 342-350.

Huang, H., Du, Y. S., Yang, J., Huang, H., Tao, P., Huang, Z. et al., 2013. Geochemistry of the Late Paleozoic cherts in the

Youjiang Basin: Implications for the basin evolution. J. Palaeogeog., 2, 402–421.

Hussain, M. F. and Dey, A., 2022. Geochemical characteristics of mafic intrusive rocks from the Naga Hills Ophiolite, north-east India: Constraints on petrogenesis and tectonic setting. Geol. J., 57, 5222-5238.

Imtisunep, S., Singh, A. K., Bikramaditya, R., Khogenkumar, S., Chaubey, M. and Kumar, N., 2022. Evidence of intraplate magmatism and subduction magmatism during the formation of Nagaland–Manipur Ophiolites, Indo–Myanmar Orogenic Belt, north-east India. Geol. J., 57, 782-800.

Jochum, K. P., Weis, U., Schwager, B., Stoll, B., Wilson, S. A., Haug, G. H., Andreae, M.O, and Enzweiler, J., 2016. Reference values following ISO guidelines for frequently requested rock reference materials. Geostandards and Geoanalytical Res.40, 333-350.

Jones, B. and Manning, D. A., 1994. Comparison of geochemical indices used for the interpretation of palaeoredox conditions in ancient mudstones. Chem. geol., 111, 111-129.

Kacker, R. and Roy, R., 1980. Geology and mineral resources of naga hills orogenic belt in a tethyan domain along eastern peri-indian suture. A preliminary geological synthesis.

Kato, Y., Nakao, K. and Isozaki, Y., 2002. Geochemistry of Late Permian to Early Triassic pelagic cherts from southwest Japan: Implications for an oceanic redox change. Chem. Geol., 182, 15–34

Khogenkumar, S., Singh, A. K., Kumar, S., Lakhan, N., Chaubey, M., Imtisunep, S., Dutt A. and Oinam, G., 2021. Subduction versus non-subduction origin of the Nagaland-Manipur Ophiolites along the Indo-Myanmar Orogenic Belt, northeast India: Fact and fallacy. Geol. J., 56, 1773-1794.

Kiliç, G., Selman Aydoğan, M. and Kumral, M., 2018. Preliminary results of the radiolarian-chert hosted manganese deposit within the Vezirler ophiolitic mélange (Kula-Manisa, western Turkey): constraints on the origin, paleo-redox conditions, and depositional environments. Arab. J. Geosc., 11, 1-22.

Krishna, A. K., Murthy, N. N. and Govil, P. K., 2007. Multielement analysis of soils by wavelength-dispersive X-ray fluorescence spectrometry. Atomic Spectroscopy-Norwalk Connecticut, 28, 202.

Mathur, L. P., and Evans, P., 1964. Oil in India. Int. Geol. Cong. 22nd Session, New Delhi.

Murray, R. W., 1994. Chemical criteria to identify the depositional environment of chert: General principles and applications. Sed. Geol., 90, 213–232.

Murray, R. W., Buchholtz Ten Brink, M. R., Jones, D. L., Gerlach, D. C. and Russ, G. P., 1990. Rare earth elements as indicators of different marine depositional environments in chert and shale. Geol., 18, 268–271.

Ningthoujam, P. S., Dubey, C. S., Guillot, S., Fagion, A. S. and Shukla, D. P., 2012. Origin and serpentinization of ultramafic rocks of Manipur Ophiolite Complex in the Indo-Myanmar subduction zone, Northeast India. J. Asian Earth Sci., 50, 128-140.

Nozaki, Y., Zhang, J. and Amakawa, H., 1997. The fractionation between Y and Ho in the marine environment. Earth Planet. Sci. Lett.,148, 329–340

Owen, A. W., Armstrong, H. A. and Floyd, J. D., 1999. Rare earth element geochemistry of upper Ordovician cherts from the Southern Uplands of Scotland. J. Geol. Soc., 156, 191-204.

Rao, B. V., Ezung, C. and Nayak, R., 2010. Geology, genesis and tectonic setting of volcanic rocks from Naga Ophiolite belt. Geol. Soc. India. Mem., 75, 317–327.

Robertson, A. H., 2002. Overview of the genesis and emplacement of Mesozoic ophiolites in the Eastern Mediterranean Tethyan region. Lithos, 65, 1-67.

Saha, A., Santosh, M., Ganguly, S., Manikyamba, C., Ray, J. and Dutta, J., 2018. Geochemical cycling during subduction initiation: Evidence from serpentinized mantle wedge peridotite in the south Andaman ophiolite suite. Geoscience Frontiers, 9, 1755-1775.

Saha, A., Mudholkar, A. V., Kamesh Raju, K. A., Doley, B. and Sensarma, S., 2019. Geochemical characteristics of basalts from Andaman subduction zone: Implications on magma genesis at intraoceanic back-arc spreading centres. Geol. J., 54, 3489-3508

Sengupta, S., Acharyya, S. K., Van Den Hul, H. J. and Chattopadhyay, B., 1989. Geochemistry of volcanic rocks from the Naga Hills ophiolites, northeast India and their inferred tectonic setting. J. Geol. Soc., 146, 491-498.

Singh, A. K., Khogenkumar, S., Singh, L. R., Bikramaditya, R. K., Khuman, C. M. and Thakur, S. S., 2016. Evidence of Mid-ocean ridge and shallow subduction forearc magmatism in the Nagaland-Manipur ophiolites, northeast India: constraints from mineralogy and geochemistry of gabbros and associated mafic dykes. Geochemistry, 76, 605-620.

Sun, S. S. and McDonough, W. F., 1989. Chemical and isotopic systematics of oceanic basalts: implications for mantle composition and processes. Geol. Soc., London, Special Publications, 42, 313-345.

Taylor, S. R. and McLennan, S. M., 1985. The continental crust: Its composition and evolution. Oxford: Blackwell Scientific

Taylor, S. R. and McLennan, S. M., 1995. The geochemical evolution of the continental crust. Rev. geophys., 33, 241-265.

Thong, G. T., Imchen, W., and Walling, T., 2022. Geochemical evidences on the origin and paleo-oceanic depositional setting of the Naga Hills Ophiolite cherts, North East India. Geol. J., 57, 3114-3134.

Verencar, A., Saha, A., Ganguly, S. and Manikyamba, C., 2021. Tectono-magmatic evolution of Tethyan oceanic lithosphere in supra subduction zone fore arc regime: Geochemical fingerprints from crust-mantle sections of Naga Hills Ophiolite. Geosci. Frontier, 12, 101096.

Verencar, A., Saha, A., Ganguly, S., Satyanarayanan, M., Doley, B., and Mohan, M. R., 2022. Multistage melt impregnation in Tethyan oceanic mantle: Petrochemical constraints from channelized melt flow in the Naga Hills Ophiolite. Geochem., 82(1), 125821.

Verencar, A., Saha, A., Ganguly, S., Satyanarayanan, M. and Mohan, M. R., 2024a. Geochemical dichotomy of Tethyan oceanic mantle and the supercontinent connection: Insights from Os isotopic signatures of mantle peridotites from Naga Hills ophiolite. Gond. Res., 128, 424-438.

Verencar, A., Saha, A., Sorcar, N., Ganguly, S., Kumar, P. and Singh, A. K., 2024b. Hydro-uvarovite from Mantle Peridotites of Naga Hills Ophiolite: A Mineral Tracer for Neo-Tethyan

Mantle Wedge Metasomatism. Acta Geologica Sinica-English Edition, 98, 867-877.

Vidyadharan, K. T., Joshi, A., Ghose, S., Gaur, M. P., Sukla, R. and Ghose, N. C., 1989. Manipur ophiolites: its geology, tectonic setting and metallogeny. Phanerozoic Ophiolites of India, Suman Publ, 197-212.

Wang, J., Chen, D., Wang, D. A. N., Yan, D., Zhou, X. and Wang, Q., 2012. Petrology and geochemistry of chert on the marginal zone of Yangtze Platform, western Hunan, South China, during the Ediacaran–Cambrian transition. Sedimentology, 59(3), 809-829.

Yamamoto, K.,1983. Geochemical study of Triassic bedded cherts from Kamiaso, Gifu Prefecture. J. Geol. Soc. Jap., 89, 143–162.

Zhang, C., Gao, S., Zhang, G., Guo, A., Yuan, H., Liu, X. and Wang, J., 2004. Geochemistry of ophiolite cherts from the Qinling orogenic belt and implications for their tectonic settings. Science in China Series D: Earth Sci., 47, 329-337.

Appendix 1. Trace and REE analyses of Certified Reference Material

Sample	JB2			JA 1		
(ppm)	Observed values (n=3)	RSD	Reported values	Observed values (n=3)	RSD	Reported values
Cr	27.0	0.35	26.7	5.38	16.9	7.50
Co	36.9	0.78	37.6	10.7	1.93	11.5
Ni	14.7	1.15	14.8	3.16	9.06	2.20
Rb	5.94	0.28	6.40	9.54	1.67	11.0
Sr	179	1.16	178	254	2.17	259
Cs	0.70	1.48	0.80	0.56	1.22	0.63
Ba	218	0.52	218	305	1.38	304
Sc	53.6	1.04	54.1	26.5	0.48	27.9
V	574	9.86	572	83.5	2.47	106
Ta	0.03	6.40	0.04	0.09	0.73	0.10
Nb	0.46	4.44	0.57	1.21	1.23	1.33
Zr	47.2	2.28	48.3	83.3	0.53	83.7
Hf	1.48	1.12	1.49	2.58	0.43	2.51
Th	0.23	4.62	0.26	0.73	2.39	0.76
U	0.14	2.88	0.15	0.32	2.53	0.34
Y	22.4	2.03	23.6	26.9	0.31	28.0
Li	8.08	2.34	8.08	10.5	0.81	10.4
La	2.10	1.92	2.28	4.63	1.57	4.88
Ce	5.85	0.94	6.55	12.1	0.86	13.2
Pr	1.03	2.79	1.13	1.89	1.02	2.08
Nd	5.83	1.73	6.39	9.98	0.73	10.7
Sm	2.15	1.88	2.27	3.25	0.17	3.40
Eu	0.77	1.67	0.84	1.00	1.18	1.11
Gd	3.04	1.97	3.12	3.96	0.89	4.15
Tb	0.51	1.58	0.59	0.63	1.06	0.73
Dy	3.57	0.36	3.87	4.29	1.97	4.75
Ho	0.77	2.27	0.86	0.90	2.19	1.03
Er	2.34	2.24	2.54	2.68	1.52	2.96
Tm	0.35	3.28	0.39	0.39	0.42	0.45
Yb	2.33	2.02	2.53	2.65	1.54	2.95
Lu	0.36	4.02	0.39	0.41	1.27	0.45
Cu	212	1.00	222	42.60	2.47	42.5
Pb	7876	2.31	5.25	8296	2.99	5.86
Zn	94.3	2.50	110	65.58	8.27	88.3
Ga	30.5	1.33	16.6	36.43	2.38	16.7

Reported values from Jochum et al. (2016)

Received on: 02-12-2024; Revised on: 18-02-2025 ; Accepted on: 28-02-2025